remote sensing

MDPI

Article

Biomass Estimation of Milk Vetch Using UAV Hyperspectral Imagery and Machine Learning

Hao Hu [1,2], Hongkui Zhou [1,2], Kai Cao [3], Weidong Lou [1,2], Guangzhi Zhang [4], Qing Gu [1,2] and Jianhong Wang [3,*]

[1] Institute of Digital Agriculture, Zhejiang Academy of Agricultural Sciences, Hangzhou 310021, China; huh@zaas.ac.cn (H.H.); zhouhongkui@zaas.ac.cn (H.Z.); louwd@zaas.ac.cn (W.L.); guq@zaas.ac.cn (Q.G.)
[2] Key Laboratory of Information Traceability for Agricultural Products, Ministry of Agriculture of China, Hangzhou 310021, China
[3] Institute of Environment, Resource, Soil and Fertilizer, Zhejiang Academy of Agricultural Sciences, Hangzhou 310021, China; caokai@zaas.ac.cn
[4] Zhejiang Institute of Hydraulics and Estuary, Hangzhou 310020, China; guangzhi0125@163.com
* Correspondence: wangjh@zaas.ac.cn

Abstract: Milk vetch (*Astragalus sinicus* L.) is a winter-growing plant that can enhance soil fertility and provide essential nutrients for subsequent season crops. The fertilizing capacity of milk vetch is closely related to its above-ground biomass. Compared to the manual measurement methods of milk vetch biomass, remote sensing-based estimation methods have the advantages of rapid, noninvasive, and large-scale measurement. However, few studies have been conducted on remote sensing-based estimation of milk vetch biomass. To address this shortcoming, this study proposes combining unmanned aerial vehicle (UAV)-based hyperspectral imagery and machine learning algorithms for accurate estimation of milk vetch biomass. Through the analysis of hyperspectral images and feature selection based on the Pearson correlation and principal component analysis, vegetation indices (VIs), including near-infrared reflectance (NIR), red-edge spectral transform index (RE), and difference vegetation index (DVI), are selected as estimation metrics of the model development process. Four machine learning methods, including random forest (RF), multiple linear regression (MLR), deep neural network (DNN), and support vector machine (SVM), are used to construct the biomass models. The results show that the RF estimation model exhibits the highest coefficient of determination (R^2) of 0.950 and the lowest relative root-mean-squared error (RRMSE) of 14.86% among all the models. Notably, the DNN model demonstrates promising performance on the test set, with the R^2 and RRMSE values slightly superior and inferior to those of the RF, respectively. The proposed method based on UAV imagery and machine learning can provide an accurate and reliable large-scale estimation of milk vetch biomass.

Keywords: UAV; milk vetch; above-ground biomass; hyperspectral imagery; machine learning

Citation: Hu, H.; Zhou, H.; Cao, K.; Lou, W.; Zhang, G.; Gu, Q.; Wang, J. Biomass Estimation of Milk Vetch Using UAV Hyperspectral Imagery and Machine Learning. *Remote Sens.* **2024**, *16*, 2183. https://doi.org/10.3390/rs16122183

Academic Editor: Dusan Gleich

Received: 3 May 2024
Revised: 3 June 2024
Accepted: 13 June 2024
Published: 16 June 2024

1. Introduction

Milk vetch (*Astragalus sinicus* L.) is a green manure, a cover crop, that grows in the winter season [1,2]. Milk vetch has been widely cultivated in East Asian countries, such as China, Japan, and Korea [3]. The growth of milk vetch in the following winter times can fully use the light, water, heat, and other natural resources and can input nitrogen nutrition into the agroecosystem through biological nitrogen fixation [4]. Under phosphorus-deficient soil conditions, the root of milk vetch secretes organic acids, which can increase the availability of anionic nutrients, such as phosphorus [5], thus increasing phosphorus effectiveness. The decomposition of milk vetch residues returns potassium to the field in a soluble form, which increases the available soil potassium pool for subsequent uptake by rice [6]. In addition, milk vetch can also improve soil fertility and aeration by reducing soil bulk density [7], thus enhancing microbial and enzymatic activities in soil. Residues of milk vetch in the soil can free a lot of nutrients for the subsequent crop, which

can be helpful in obtaining a high yield [8]. Further, milk vetch can also be used as a forage grass, honey, and medicine [3].

The effect of milk vetch on soil fertility and crop yield mainly depends on the amount of its above-ground fresh biomass. Usually, the fresh biomass of milk vetch can reach its highest value at the full flowering stage [9]. Destructive sampling is the traditional approach for obtaining a milk vetch biomass. This approach requires manual cutting, weighing, and recording, which consumes much time and labor. With the recent development of sensors, remote sensing has been regarded as the best tool for plant biomass estimation. Recent studies have shown that satellite remote sensing can be a good data source for large-scale estimation of various plant biomasses [10]. However, the satellite remote-sensing methods can be easily disturbed by weather, satellite visit time, and other factors.

Unmanned aerial vehicles (UAVs) have been developed rapidly in recent years. Compared to satellites, UAVs have the advantage of providing near-Earth information with a high spatiotemporal resolution and easily controlled flight [11]. A UAV as a platform combined with spectral sensors has become an efficient method for biomass estimation of various crops. Good results were obtained for maize [12,13], rice [14], barley [15,16], wheat, and grass [17]. In the related studies, a variety of vegetative indices (VIs), including the normalized difference vegetation index (NDVI) [18], green normalized differential vegetation index (GNDVI) [18], and triangular vegetation index (TVI) [19], were used for biomass estimation. Machine learning can be defined as an artificial intelligence concerned with statistical algorithms that can learn from black box data [20]. In recent years, machine learning has been widely applied to the agricultural field, and it has been proven that machine-learning methods could help improve the accuracy of VI-based biomass models [21].

Numerous studies on crop biomass estimation using remote sensing have been conducted in recent years. However, there have been fewer studies on using VIs obtained from a UAV hyperspectral imager in combination with machine learning-based methods for milk vetch biomass estimation. To address this shortcoming, this study defines the following objectives: (1) investigate the feasibility of using UAV hyperspectral imaging to estimate milk vetch biomass, (2) use the optimal spectral VIs as model input parameters, and (3) compare the performance of different machine-learning based milk vetch estimation biomass models. Accordingly, a milk vetch biomass estimation field experiment using UAVs and machine learning methods was conducted, and the feasibility of the study and the model performance were analyzed. These findings will be valuable and helpful in the development of the milk vetch industry.

2. Materials and Methods

2.1. Study Area and Experimental Design

The test site was located at the experimental field base of the Zhejiang Academy of Agricultural Sciences (ZAAS), Xiangxi town, Lanxi City, Zhejiang Province, China, as shown in Figure 1A. The climate of this area belongs to the subtropical monsoon region of East Asia, with an average monthly temperature of 17.6 °C, a monthly precipitation of 1476.5 mm, an annual average relative humidity of 76.5%, and an annual average frost-free period of 264 days. The farmland was a wasteland before it was cultivated in October 2021. The sandy soil in the field had poor fertility, with an average organic matter content of 0.152 g/kg. Uneven fertility was observed, and the growth of spatial heterogeneity in milk vetch in the field is shown in Figure 1. The field was 157.0 m long and 63.0 m wide. Milk vetch was seeded on 5 November 2021 and 8 November 2022. The planting density was 5.0×10^5/ha. In total, 82 milk vetch samples were freshly cut on 12 April 2022, and 100 samples were cut on April 10, 2023. The average canopy coverages during the sampling period were 0.85 and 0.90, respectively. The sampling area was 0.25 m^2. The sampling position was captured by GPS, and the above-ground biomass of milk vetch was weighed after the cut.

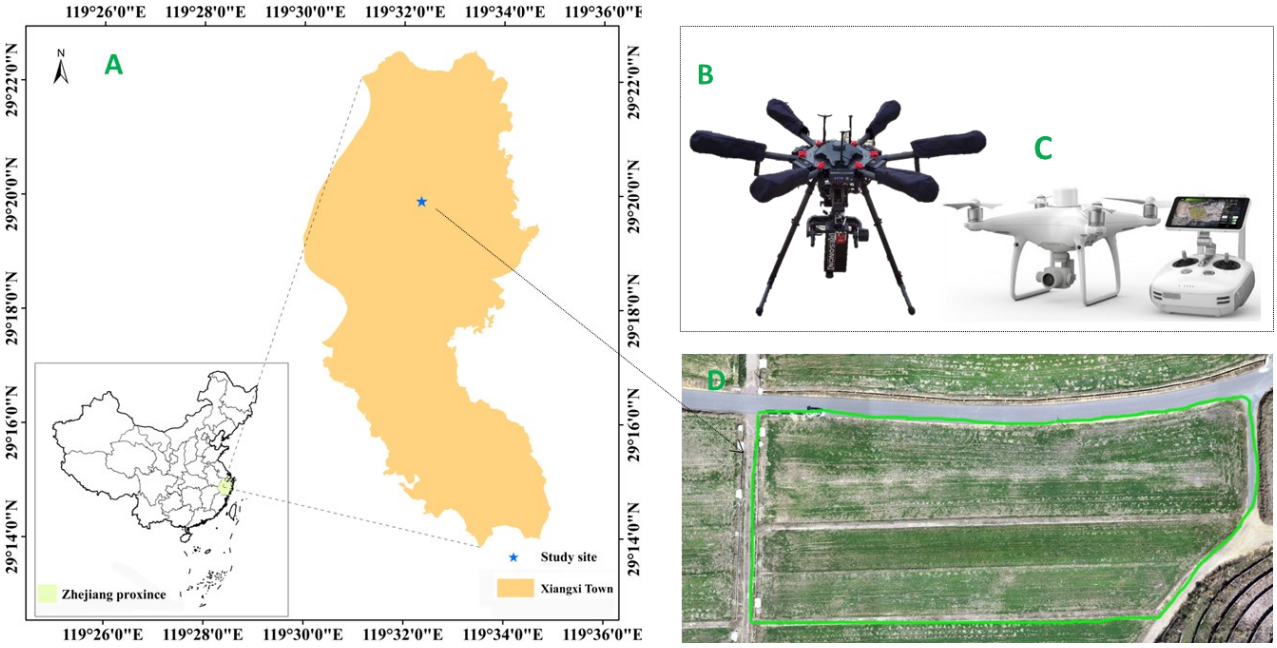

Figure 1. Study area (**A**,**D**) and a UAV used in this study; (**B**): DJI Matrice 600 Pro equipped with a Pika XC2 hyperspectral imager; (**C**): DJI Phantom 4 RTK.

2.2. UAV Image Data Collection and Analysis

On the sampling days (12 April 2022, and 10 April 2023) and before the milk vetch was cut, a DJI Matrice 600 Pro drone (DJI, Shenzhen, China) equipped with a Pika XC2 hyperspectral sensor (Resonon, Bozeman, MT, USA); Figure 1C was used to collect the milk vetch hyperspectral images from 11:00 am to 12:30 pm under clear and cloudless weather conditions. The flight activities were conducted at an altitude of 100 m. The hyperspectral images were calibrated by a radiation-calibrated standard tarp that was placed flat on the ground in the flight area.

Simultaneously, a DJI Phantom 4 RTK was used to collect RGB images. The flight height was set 100 m, and the forward and side overlaps of the visible images were set to 70% and 80%, respectively. The RGB sensor has 20 million effective pixels per inch. And the spatial resolution of RGB image was 0.71 cm. The RGB images were used to assist in hyperspectral image geometric correction and the manual delineation of plant crowns. The collected hyperspectral images with a spatial resolution of 5.0 cm included spectral bands from 400 nm to 1000 nm and had a spectral resolution of 1.3 nm, 447 spectral channels, and 1600 spatial channels with a 12-bit depth. The images were stored on a memory card. The reflectance value of the milk vetch was extracted from the hyperspectral images using Software SpectrononPro (www.resonon.com (accessed on 10 June 2019). According to the previous studies, 10 spectral VIs were calculated, as shown in Table 1.

Table 1. Summary of the spectral VIs used in this study.

Indices	Calculation Equation	Reference
NIR	$R860$	/
RE	$R750/R710$	[22]
NDVY	$(R560 - R450)/(R560 + R450)$	[23]
CIre	$R800/R720 - 1$	[24]
CIgreen	$R800/R550 - 1$	[24]
RVI	$R800/R670$	[25]
DVI	$R800 - R670$	[26]
RDVI	$[\text{NDVI} \times (R800 + R670)^2]^{0.5}$	[27]
TVI	$0.5 \times (120 \times (R750 - R550) - 200 \times (R670 - R550)$	[28]

Table 1. *Cont.*

Indices	Calculation Equation	Reference
BNDVI	$(R860 - R450)/(R860 + R450)$	[29]
ENDVI	$[(R860 + R550) - 2 \times R450]/[R860 + R550) + 2 \times R450]$	[30]

Rx refers to the leaf reflectance at a wavelength x in nanometers; NIR is the near-infrared reflectance; RE is red-edge spectral transform index; NDVY is the normalized yellow difference vegetation index; CIre is the red-edge chlorophyll index; CIgreen is the green chlorophyll index; RVI is the ratio vegetation index; DVI is the difference vegetation index; RDVI is the ratio difference vegetation index; TVI is triangular vegetation index; BNDVI is the blue normalized difference vegetation index; ENDVI is the enhanced normalized difference vegetation index.

To select appropriate VIs to develop a biomass estimation model, this study conducted Pearson's correlation analysis and principal component analysis (PCA) to reduce the dimension and number of VIs. The two-tailed test with $p < 0.01$ was conducted during the correlation analysis between the VIs and milk vetch biomass. After the correlation analysis, the PCA with two principal components was performed, and the scores were calculated using Origin 2022. According to the calculated scores, the VIs with a close relationship with milk vetch biomass were obtained.

2.3. Model Construction and Test

The flowchart of the entire process, from image acquisition to data reduction and modeling, is shown in Figure 2. Before modeling, all input variables were standardized by

$$x_n = \frac{x_i - x_{\min}}{x_{\max} - x_{\min}} \quad (1)$$

where x_n is the normalized value, and $x_{\max}$ and $x_{\min}$ are the maximum and minimum values, respectively.

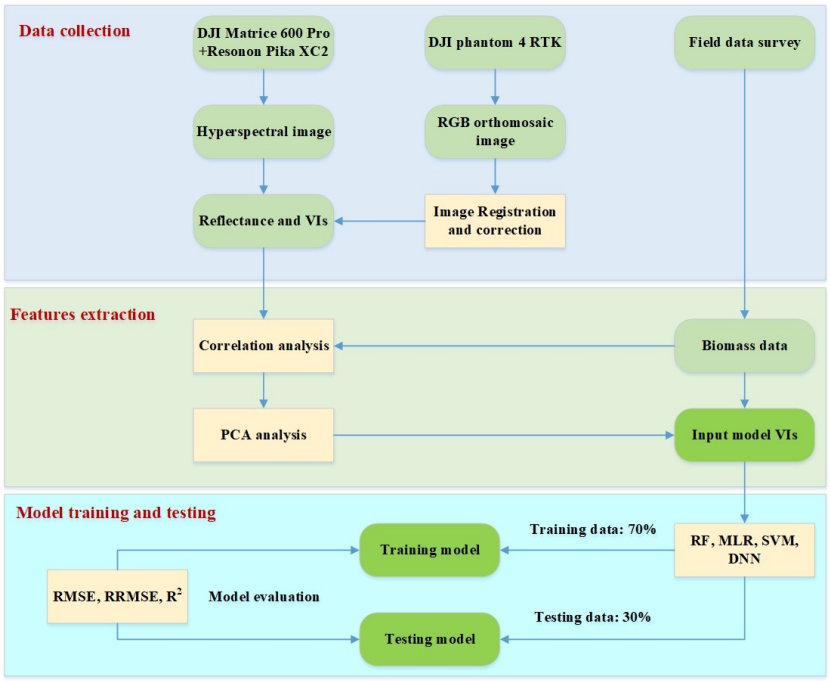

Figure 2. Design workflow of the biomass estimation model.

In this study, a total of 82 and 100 samples collected in 2022 and 2023 were used, of which, two-thirds were used for model training, and the remaining one-third was used independently for model testing. Four machine learning regression methods, including the random forest (RF), multiple linear regression (MLR), support vector machine (SVM), and deep neural network (DNN), were used to construct the milk vetch biomass estimation

model. RF is a commonly used machine learning algorithm, that combines the output of multiple decision trees to reach a single result. It can handle regression problems easily. In the RF method, the number of decision trees was set to 500, and the other parameters were set to the RF algorithm's default parameters. MLR is a traditional modeling method and often used to determine a mathematical relationship among several random variables. In the MLR analysis, "enter" denoted the model input method. SVM is commonly used for regression analysis due to its powerful supervised learning algorithms. In the SVM method, default parameters were used.

DNN is a machine learning technique that allows a computer, by training it, to do tasks that would be very difficult to do using conventional techniques. The DNN model's structure used in this study is shown in Figure 3. The input layer of the DNN model consisted of the selected features and contained four hidden layers, with 256, 128, 64, and 32 neurons, respectively. The output layer provided the biomass data. The ReLU activation function was used after each hidden layer. After the first hidden layer, a dropout layer with a ratio of 0.1 was used to reduce the model overfitting effect. The Adaptive Moment Estimation (Adam) optimizer was employed to train the network. The maximum number of training iterations was set to 500, and the mini-batch size was 256. The initial learning rate was 0.001, with a 10% decrease at every 100 rounds.

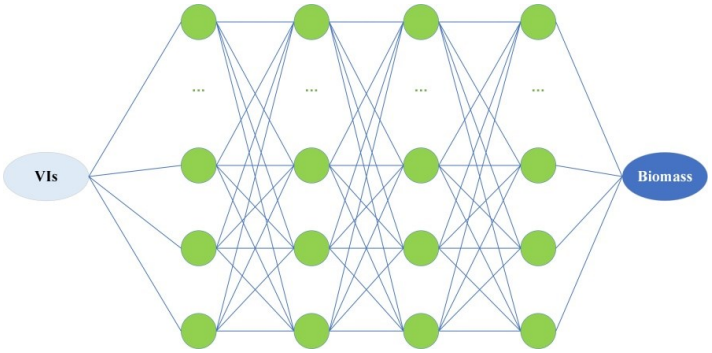

Figure 3. DNN network structure used in this study.

The training and test performances of the models were evaluated using the coefficient of determination (R^2), root-mean-square error (RMSE), and relative root-mean-squared error (RRMSE), which were, respectively, calculated by

$$R^2 = \frac{\sum_{i=1}^{n}(x_i - \overline{x})^2(y_i - \overline{y})^2}{\sum_{i=1}^{n}(x_i - \overline{x})^2 \sum_{i=1}^{n}(y_i - \overline{y})^2}, \quad (2)$$

$$RMSE = \sqrt{\frac{1}{N}\sum_{i=1}^{N}(x_i - y_i)^2}, \quad (3)$$

$$RRMSE = \frac{\sqrt{\frac{1}{N}\sum_{i=1}^{N}(x_i - y_i)^2}}{\overline{x}} \times 100\%, \quad (4)$$

where x and y are the measured and estimated values, respectively; $\overline{x}$ and $\overline{y}$ denote the average values of measured and estimated biomass, respectively; and N is the number of observations.

2.4. Data Analysis

The Pearson correlation with a two-tailed test between the VIs and biomass, the fitted linear regression of the measured and machine-learning estimated biomass, and the PCA

of the 10 VIs were analyzed using IBM SPSS Statistics 25.0 (SPSS Inc., New York, NY, USA, 2017). The correlation, scatter, fitted line, and PCA plots shown in the following section were drawn by Origin 2022 (Origin Lab Corporation, Northampton, MA, USA, 2022). The machine learning algorithms, including RF, DNN, SVM, and MLR, were run in MATLAB R2022a software (The MathWorks, Inc., Torrance, CA, USA, 2022).

3. Results

3.1. Milk Vetch Biomass

The biomass values of milk vetch in 2022 and 2023 are shown in Table 2. In 2022, the minimum and maximum values of the milk vetch biomass were 0.264 kg/m^2 and 12.39 kg/m^2, respectively, and the average biomass value was 4.806 kg/m^2. The coefficient of variance (CV) of milk vetch was 0.756, which indicated significant changes in the biomass value. The minimum and maximum biomass values in 2023 were 0.372 kg/m^2 and 6.38 kg/m^2, respectively, and the average biomass value was 2.36 kg/m^2. The CV of milk vetch biomass in 2023 was 0.631. In 2023, the biomass value had a smaller range and CV than in 2022.

Table 2. Biomass (kg/m^2) of milk vetch in 2022 and 2023.

Year	Number of Samples	Min [1]	Max [2]	Mean	CV
2022	82	0.264	12.39	4.81	0.756
2023	100	0.372	6.38	2.36	0.631

[1] Min: minimum; [2] Max: maximum.

3.2. Correlations between VIs and Milk Vetch Biomass

The correlations between the milk vetch biomass and VIs in 2022 and 2023 are shown in Figure 4. All the VIs had a significant relationship with the milk vetch biomass across the two years. In 2022, the NIR, RE, and DVI had the highest correlation coefficients of 0.837, 0.822, and 0.806 among all VIs. In 2023, NIR, RE, DVI, RDVI, and TVI were higher than the other VIs, and they were all higher than 0.800. Finally, the correlation coefficient in 2023 was higher than in 2022. The VIs including NIR, RE, CIre, CIgreen, DVI, RDVI, and TVI which had correlation coefficients of higher than 0.600 were selected for further PCA analysis.

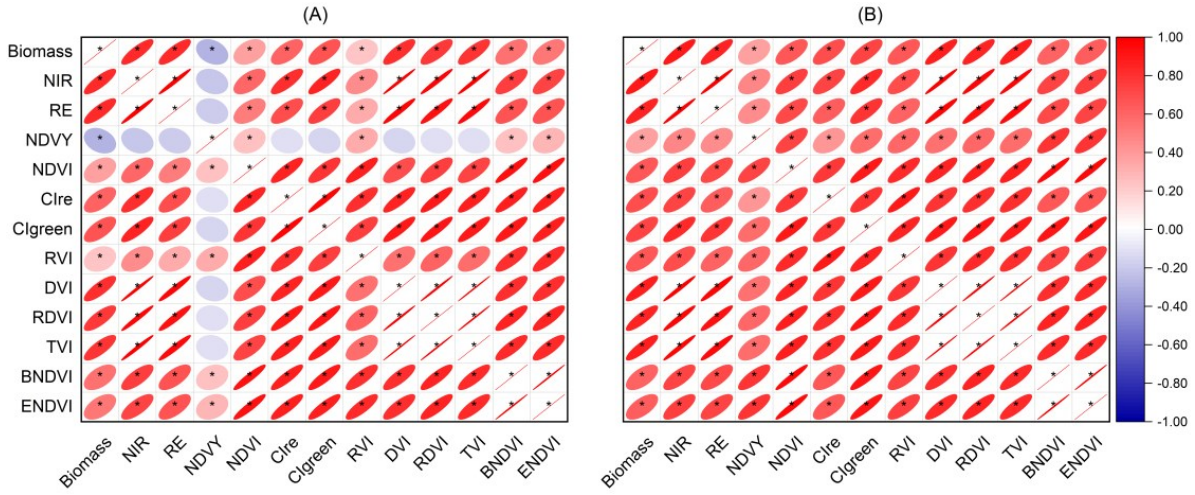

Figure 4. Correlations between the VIs and milk vetch biomass in 2022 (**A**) and 2023 (**B**). * indicates significant at $p < 0.05$ with two-tailed test.

3.3. PCA of VIs

Using highly correlated variables as input data for a prediction model might cause multi-collinearity problems. In addition, using too many VIs as input parameters in the

biomass evaluation model design might make the model complex and difficult to construct. However, the PCA can be used to avoid these problems. The results for 2022 and 2023 are shown in Figures 5A and 5B, respectively. As presented in Figure 4A, the RE, NIR, and DVI had the closest relationship and load score with the milk vetch biomass among all VIs. The same result could be observed for 2023, as shown in Figure 5B. Therefore, the RE, NIR, and DVI were selected as input VIs to design a milk vetch biomass evaluation model.

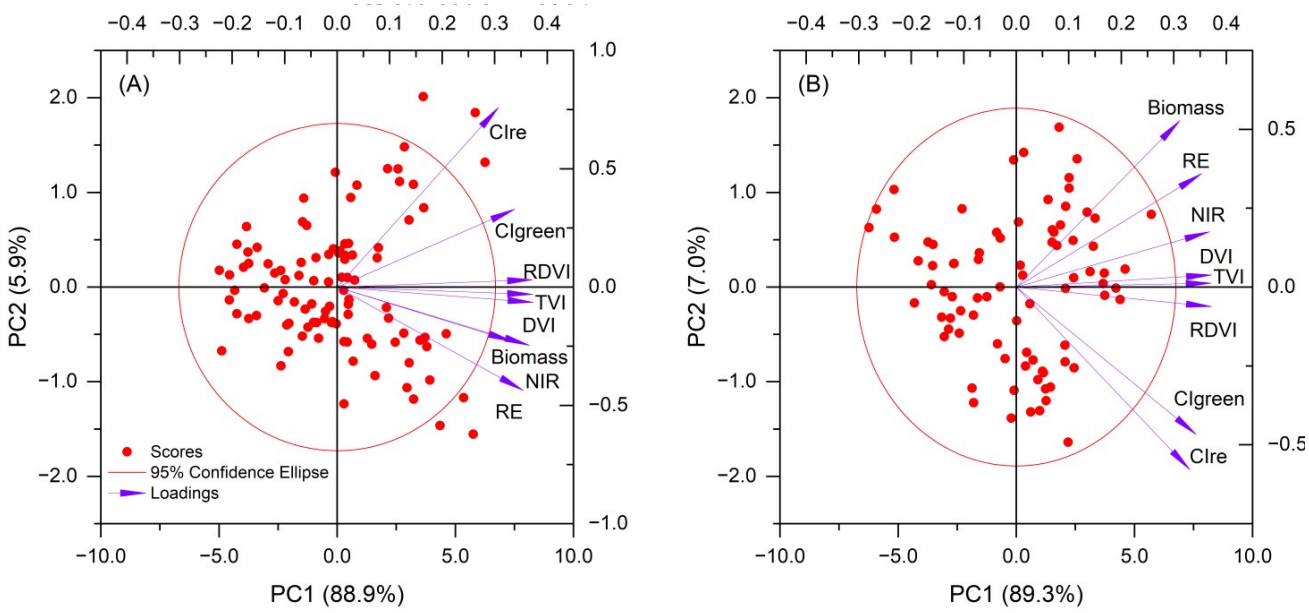

Figure 5. PCA plots of the milk vetch VIs in 2022 (**A**) and 2023 (**B**).

3.4. Performance of Milk Vetch Biomass Evaluation Models

The RF, MLR, DNN, and SVM models were used to construct a biomass estimation model of milk vetch. The results are presented in Table 3 and Figure 6. In 2022, the RF model had the highest coefficient of determination (R^2) and the smallest RMSE and RRMSE on both training and test sets among all models; the SVM model had the lowest R^2 and the highest RMSE and RRMSE values among all models; and the DNN and MLR were ranked as the second and third after the RF model. In 2023, among all the models, the RF model had the highest R^2, and the SVM model had the lowest R^2 on the training set; on the test set, the DNN model had the highest R^2.

Table 3. The training and test performances of different estimation models of milk vetch.

Year	Model	Training			Test		
		RMSE (kg/m^2)	RRMSE (%)	R^2	RMSE (kg/m^2)	RRMSE (%)	R^2
2022	RF	0.833	17.71	0.950	1.651	33.01	0.793
	MLR	1.725	36.66	0.771	2.060	41.19	0.677
	SVM	1.848	39.27	0.744	2.175	43.50	0.644
	DNN	1.496	31.79	0.838	1.942	38.84	0.716
2023	RF	0.343	14.86	0.946	0.807	32.94	0.759
	MLR	0.643	27.86	0.795	0.734	29.96	0.792
	SVM	0.650	28.17	0.790	0.733	29.91	0.797
	DNN	0.624	27.05	0.820	0.733	29.90	0.813
2022 + 2023	RF	0.634	19.09	0.955	1.758	47.17	0.700
	MLR	1.425	42.90	0.758	1.604	43.03	0.711
	SVM	1.513	45.57	0.744	1.677	44.10	0.700
	DNN	1.343	40.43	0.798	1.625	43.59	0.701

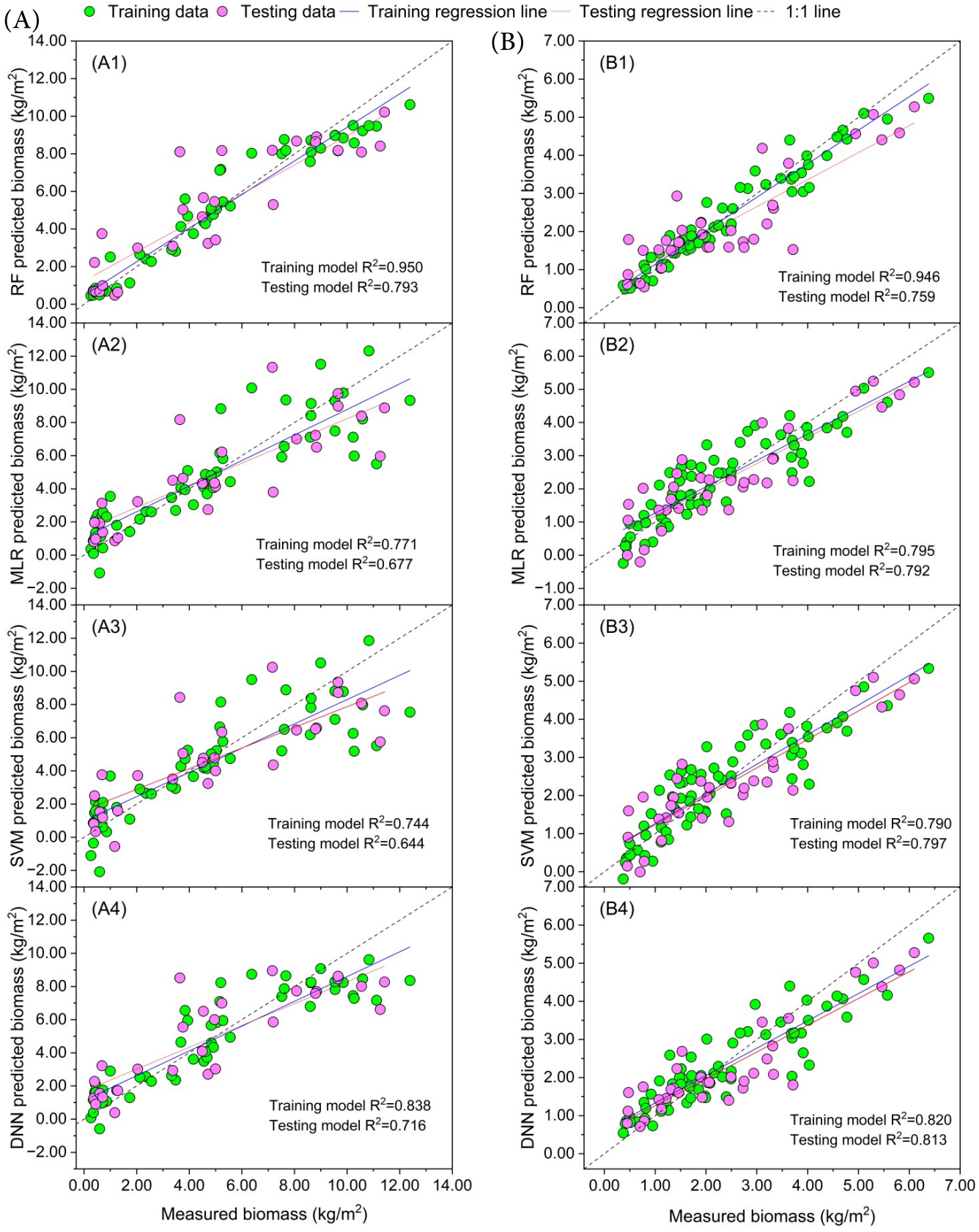

Figure 6. Training and test results of milk vetch in 2022 (**A**) and 2023 (**B**). A1 (B1), A2 (B2), A3 (B3), and A4 (B4) were plots of predicted biomass to measured biomass, respectively.

Regarding the RMSE and RRMSE metrics, the RF model had the lowest value on the training set but had the highest value on the test set. The data from the two years (2022 + 2023) were used to construct the estimation biomass model, and the results are shown in Table 3 and Figure 7. Compared to the models constructed using data from 2022 and 2023, the 2022 + 2023 model has a low R^2 value but slightly high RMSE and RRMSE values. The RF model had a high R^2 value on the training set for the 2022 + 2023 data compared to both 2022 and 2023 data. This proved that the RF model had excellent performance.

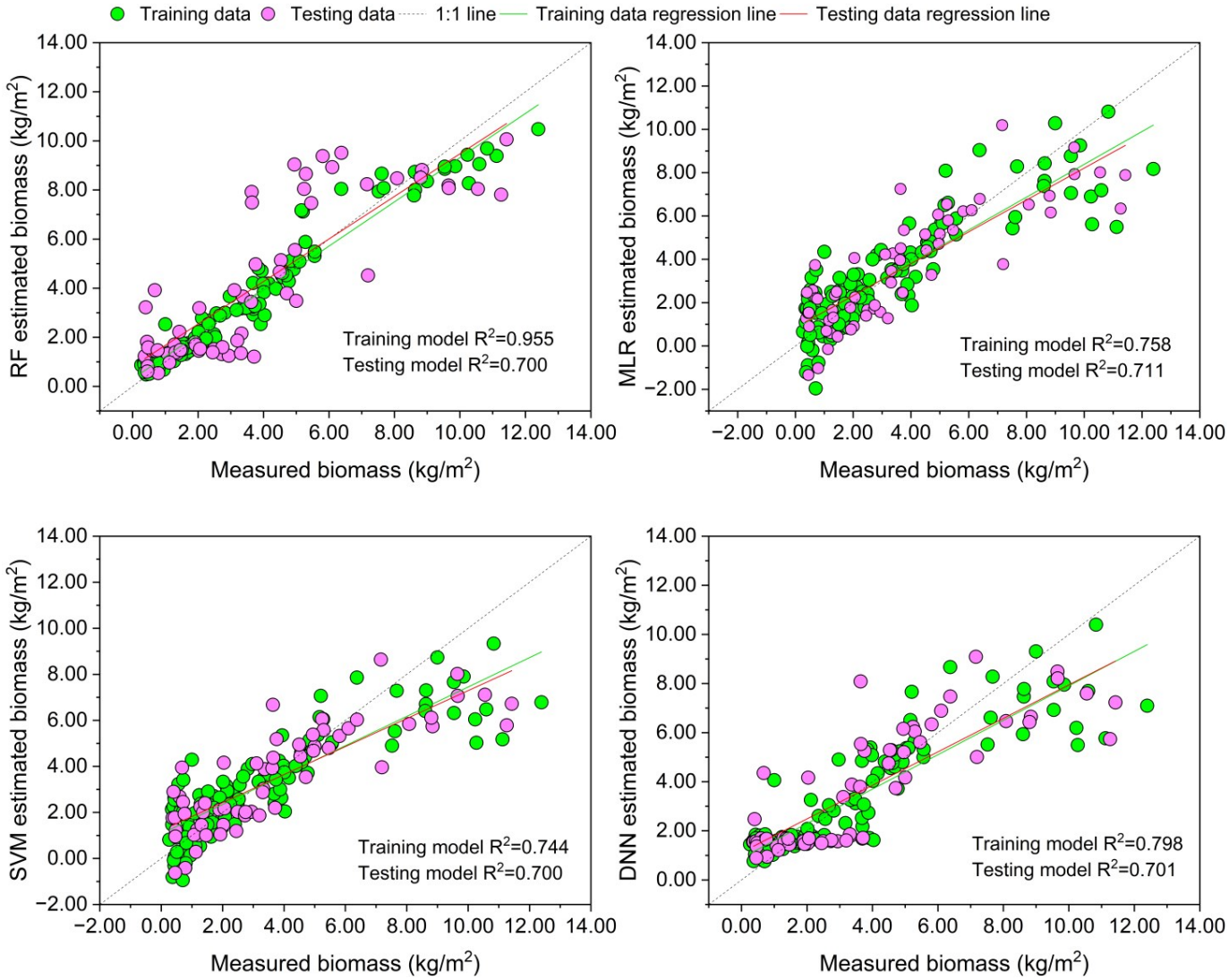

Figure 7. Training and test results of milk vetch for two-year data (2022 and 2023).

3.5. Comparison of Estimated and Measured Biomass

The violin plots shown in Figure 8A,B show the distribution of measured and machine-learning estimated milk vetch biomass values. The results indicated that the average biomass of the SVM model was almost equal to the measured value across the two years. Compared to the measured data, the shape of the biomass distributions of MLR, SVM, and DNN models indicated that the weights were highly concentrated around the median value. The biomass ranges (i.e., the max min ranges) of the SVM in 2022 and MLR in 2023 were almost near the measured ones. As shown in Figure 8, the CV of biomass was reduced when the machine learning-based model was used.

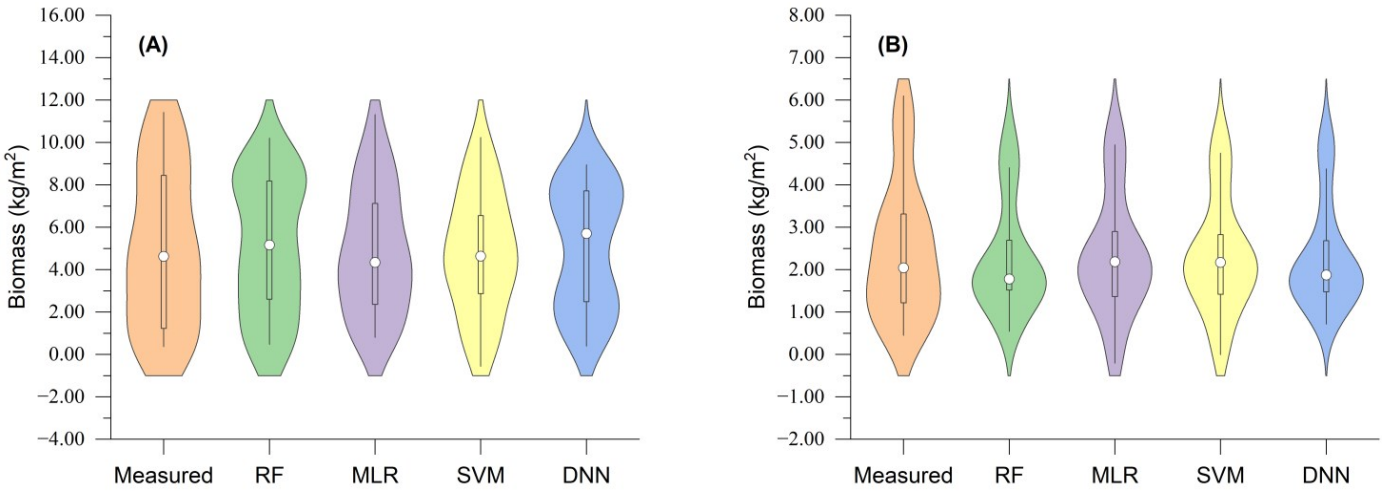

Figure 8. Estimated and measured biomass data in 2022 (**A**) and 2023 (**B**).

4. Discussion

A UAV is a suitable platform that can be used for data acquisition on a large scale in comparison with ground-based instruments. The UAV-derived imagery is geometrically registered and can provide multi-sensor data, such as spectral, thermal, and fluorescence characteristics. Many previous studies have proven that plant biomass can be estimated with excellent performance using UAVs [31–33]. In this study, hyperspectral imagery was performed using a UAV, and the hyperspectral indices were used to estimate the milk vetch biomass. The highest R^2 values on the training and test sets were 0.950 and 0.813, respectively, which suggested that UAVs could have great potential for evaluating the plant growing status in large field areas.

Hyperspectral images contain rich and spectral data, from which hundreds of VIs can be calculated. However, using all these VIs to design an estimation model might cause auto-collinearity problems. Therefore, it is necessary to reduce the amount of data used for model construction. To this end, this study analyzed the Pearson correlation of the VIs and biomass first. Then, the PCA was performed to reduce the number of input VIs. The feature screening methods proposed by Taşan et al. [34] were also employed. In addition to the Person correlation and PCA, other feature selection methods were used in previous studies [35,36]. Nevertheless, how to select the most appropriate feature screening methods for model design requires further research.

In this study, the VIs were calculated from the plant canopy reflectance that was collected by the hyperspectral imager. Many previous studies have proven that VIs are useful for estimating plant biomass [37–39]. In this study, the NIR, RE, and DVI were selected as model input parameters after the Person correlation calculation and PCA analysis. However, the VIs can be disturbed by the canopy background, bidirectional reflectance, shadows, and other factors. Some researchers have reported that combining the VIs with morphology and physiology characteristics can improve the accuracy of a biomass estimation model [33,38,40]. Still, future research is needed in this field.

The results presented in this study demonstrate the suitability of machine learning-based models, such as RF, MLR, SVM, and DNN, for biomass estimation of milk vetch plants. The results indicated that the RF model had the highest R^2 and lowest RMSE and RRMSE among all the models across the two years. A similar result was obtained by Freitas et al. [35]. The good performance of the RF model could be related to the randomness, which could minimize the correlations between decisions in the model. In general, the DNN model had the second-best performance following the RF model. However, in the experiment on the 2023 data, the R^2 and RRMSE of the DNN model on the test set were 0.813 and 29.90, respectively. They were higher than those of the RF model, which suggested that the DNN model could have great potential in biomass estimation.

The process from data collection to model development requires careful consideration and analysis. It is important to improve the quality of data obtained from UAV-based imagery, ground-based observations, and modeling approaches, which could be influenced by errors. Therefore, a standardized procedure of the above process is needed. Future work could investigate using different image collection methods, data processing algorithms, and modeling approaches for estimating biomass; also, plant biophysical properties and error sources could be further explored. Moreover, assessing the uncertainty and transferability of developed models and application testing is also needed.

This study has a few shortcomings that could be addressed in future work. First, poor soil fertility might weaken the milk vetch growth, and a small biomass was obtained. This could have a negative effect on both data quality and model building. However, it is an important and valuable point for milk vetch to use milk vetch to fertilize poor soil properties. Second, there were certain differences between the 2022 and 2023 models, and the performance of the 2022 + 2023 model decreased in comparison to the two single-year models. Therefore, developing an efficient model for practical applications requires future research.

5. Conclusions

To estimate the milk vetch biomass, which might have the potential to improve soil fertility, this study develops a milk vetch biomass estimation approach using UAV-based hyperspectral imagery acquired across two years. After feature selection using the Pearson correlation and PCA, the NIR, RE, and DVI indexes are selected to estimate model input parameters. In the model design, four machine learning-based methods, including RF, MLR, SVM, and DNN, are employed to construct a biomass model. The results show that the RF model has a higher R^2 and a lower RMSE than the other three models on the training and test sets. The R^2 and RMSE values of the DNN model on the test set are slightly higher and lower than those of the RF model, respectively. This suggests that the DNN has great potential in milk vetch biomass estimation. The results presented in this study could provide a valuable reference for accurate and reliable estimation of milk vetch biomass, which can contribute to policy and management decisions for agriculture production.

Author Contributions: Conceptualization, H.H. and J.W.; methodology, H.Z. and K.C.; software, W.L.; validation, G.Z.; formal analysis, H.H.; resources, Q.G.; data curation, H.H.; writing—original draft preparation, H.H.; writing—review and editing, J.W. All authors have read and agreed to the published version of the manuscript.

Funding: This research was funded by the China Agriculture Research System of MOF and MARA (CARS-22).

Data Availability Statement: The raw/processed data required to reproduce the above findings cannot be shared at this time as the data also form part of an ongoing study.

Acknowledgments: We are very grateful to everyone who helped in the revision process of this paper.

Conflicts of Interest: The authors declare no conflicts of interest.

References

1. Chang, D.; Gao, S.; Zhou, G.; Deng, S.; Jia, J.; Wang, E.; Cao, W. The chromosome-level genome assembly of *Astragalus sinicus* and comparative genomic analyses provide new resources and insights for understanding legume-rhizobial interactions. *Plant Commun.* **2022**, *3*, 100263. [CrossRef] [PubMed]
2. Fan, Q.; Xu, C.; Zhang, L.; Xie, J.; Zhou, G.; Liu, J.; Hu, F.; Gao, S.; Cao, W. Application of milk vetch (*Astragalus sinicus* L.) with reduced chemical fertilizer improves rice yield and nitrogen, phosphorus, and potassium use efficiency in southern China. *Eur. J. Agron.* **2023**, *144*, 126762. [CrossRef]
3. Li, Y.; Zhou, L.; Li, Y.; Chen, D.; Tan, X.; Lei, L.; Zhou, J. A nodule-specific plant cysteine proteinase, AsNODF32, is involved in nodule senescence and nitrogen fixation activity of the green manure legume *Astragalus sinicus*. *New Phytol.* **2008**, *180*, 185–192. [CrossRef] [PubMed]
4. Voisin, A.-S.; Guéguen, J.; Huyghe, C.; Jeuffroy, M.-H.; Magrini, M.-B.; Meynard, J.-M.; Mougel, C.; Pellerin, S.; Pelzer, E. Legumes for feed, food, biomaterials and bioenergy in Europe: A review. *Agron. Sustain. Dev.* **2013**, *34*, 361–380. [CrossRef]

5. Huang, Q.; Zhao, Z.; Chen, W. Effects of several low-molecular weight organic acids and phosphate on the adsorption of acid phosphatase by soil colloids and minerals. *Chemosphere* **2003**, *52*, 571–579. [CrossRef]
6. Askegaard, M.; Eriksen, J. Residual effect and leaching of N and K in cropping systems with clover and ryegrass catch crops on a coarse sand. *Agric. Ecosyst. Environ.* **2008**, *123*, 99–108. [CrossRef]
7. Wang, Y.; Liu, X.; Butterly, C.; Tang, C.; Xu, J. pH change, carbon and nitrogen mineralization in paddy soils as affected by Chinese milk vetch addition and soil water regime. *J. Soils Sediments* **2013**, *13*, 654–663. [CrossRef]
8. Lee, C.H.; Park, K.D.; Jung, K.Y.; Ali, M.A.; Lee, D.; Gutierrez, J.; Kim, P.J. Effect of Chinese milk vetch (*Astragalus sinicus* L.) as a green manure on rice productivity and methane emission in paddy soil. *Agric. Ecosyst. Environ.* **2010**, *138*, 343–347. [CrossRef]
9. Zhou, G.; Cao, W.; Bai, J.; Xu, C.; Zeng, N.; Gao, S.; Rees, R.M. Non-additive responses of soil C and N to rice straw and hairy vetch (*Vicia villosa Roth* L.) mixtures in a paddy soil. *Plant Soil* **2019**, *436*, 229–244. [CrossRef]
10. Ogungbuyi, M.G.; Guerschman, J.; Fischer, A.M.; Crabbe, R.A.; Ara, I.; Mohammed, C.; Scarth, P.; Tickle, P.; Whitehead, J.; Harrison, M.T. Improvement of pasture biomass modelling using high-resolution satellite imagery and machine learning. *J. Environ. Manag.* **2024**, *356*, 120564. [CrossRef]
11. Chen, A.; Xu, C.; Zhang, M.; Guo, J.; Xing, X.; Yang, D.; Xu, B.; Yang, X. Cross-scale mapping of above-ground biomass and shrub dominance by integrating UAV and satellite data in temperate grassland. *Remote Sens. Environ.* **2024**, *304*, 114024. [CrossRef]
12. Shu, M.; Li, Q.; Ghafoor, A.; Zhu, J.; Li, B.; Ma, Y. Using the plant height and canopy coverage to estimation maize aboveground biomass with UAV digital images. *Eur. J. Agron.* **2023**, *151*, 126957. [CrossRef]
13. Zhai, W.; Li, C.; Fei, S.; Liu, Y.; Ding, F.; Cheng, Q.; Chen, Z. CatBoost algorithm for estimating maize above-ground biomass using unmanned aerial vehicle-based multi-source sensor data and SPAD values. *Comput. Electron. Agric.* **2023**, *214*, 108306. [CrossRef]
14. Derraz, R.; Melissa Muharam, F.; Nurulhuda, K.; Ahmad Jaafar, N.; Keng Yap, N. Ensemble and single algorithm models to handle multicollinearity of UAV vegetation indices for predicting rice biomass. *Comput. Electron. Agric.* **2023**, *205*, 107621. [CrossRef]
15. Bendig, J.; Bolten, A.; Bennertz, S.; Broscheit, J.; Eichfuss, S.; Bareth, G. Estimating Biomass of Barley Using Crop Surface Models (CSMs) Derived from UAV-Based RGB Imaging. *Remote Sens.* **2014**, *6*, 10395–10412. [CrossRef]
16. Bendig, J.; Yu, K.; Aasen, H.; Bolten, A.; Bennertz, S.; Broscheit, J.; Gnyp, M.L.; Bareth, G. Combining UAV-based plant height from crop surface models, visible, and near infrared vegetation indices for biomass monitoring in barley. *Int. J. Appl. Earth Obs. Geoinf.* **2015**, *39*, 79–87. [CrossRef]
17. Sinde-González, I.; Gil-Docampo, M.; Arza-García, M.; Grefa-Sánchez, J.; Yánez-Simba, D.; Pérez-Guerrero, P.; Abril-Porras, V. Biomass estimation of pasture plots with multitemporal UAV-based photogrammetric surveys. *Int. J. Appl. Earth Obs. Geoinf.* **2021**, *101*, 102355. [CrossRef]
18. Prabhakara, K.; Hively, W.D.; McCarty, G.W. Evaluating the relationship between biomass, percent groundcover and remote sensing indices across six winter cover crop fields in Maryland, United States. *Int. J. Appl. Earth Obs. Geoinf.* **2015**, *39*, 88–102. [CrossRef]
19. Chen, J.; Gu, S.; Shen, M.; Tang, Y.; Matsushita, B. Estimating aboveground biomass of grassland having a high canopy cover: An exploratory analysis of in situ hyperspectral data. *Int. J. Remote Sens.* **2009**, *30*, 6497–6517. [CrossRef]
20. van der Meijden, S.L.; Arbous, M.S.; Geerts, B.F. Possibilities and challenges for artificial intelligence and machine learning in perioperative care. *BJA Educ.* **2023**, *23*, 288–294. [CrossRef]
21. Tian, Y.; Huang, H.; Zhou, G.; Zhang, Q.; Tao, J.; Zhang, Y.; Lin, J. Aboveground mangrove biomass estimation in Beibu Gulf using machine learning and UAV remote sensing. *Sci. Total Environ.* **2021**, *781*, 146816. [CrossRef]
22. Zarco-Tejada, P.J.; Miller, J.R.; Noland, T.L.; Mohammed, G.H.; Sampson, P.H. Scaling-up and model inversion methods with narrowband optical indices for chlorophyll content estimation in closed forest canopies with hyperspectral data. *IEEE Trans. Geosci. Remote Sens.* **2001**, *39*, 1491–1507. [CrossRef]
23. Sulik, J.J.; Long, D.S. Spectral indices for yellow canola flowers. *Int. J. Remote Sens.* **2015**, *36*, 2751–2765. [CrossRef]
24. Gitelson, A.A.; Viña, A.; Ciganda, V.; Rundquist, D.C.; Arkebauer, T.J. Remote estimation of canopy chlorophyll content in crops. *Geophys. Res. Lett.* **2005**, *32*, l08403. [CrossRef]
25. Jordan, C.F. Derivation of Leaf-Area Index from Quality of Light on the Forest Floor. *Ecology* **1969**, *50*, 663–666. [CrossRef]
26. Hadjimitsis, D.G.; Papadavid, G.; Agapiou, A.; Themistocleous, K.; Hadjimitsis, M.G.; Retalis, A.; Michaelides, S.; Chrysoulakis, N.; Toulios, L.; Clayton, C.R.I. Atmospheric correction for satellite remotely sensed data intended for agricultural applications: Impact on vegetation indices. *Nat. Hazards Earth Syst. Sci.* **2010**, *10*, 89–95. [CrossRef]
27. Haboudane, D.; Miller, J.R.; Tremblay, N.; Zarco-Tejada, P.J.; Dextraze, L. Integrated narrow-band vegetation indices for prediction of crop chlorophyll content for application to precision agriculture. *Remote Sens. Environ.* **2002**, *81*, 416–426. [CrossRef]
28. Broge, N.H.; Leblanc, E. Comparing prediction power and stability of broadband and hyperspectral vegetation indices for estimation of green leaf area index and canopy chlorophyll density. *Remote Sens. Environ.* **2001**, *76*, 156–172. [CrossRef]
29. Hancock, D.W.; Dougherty, C.T. Relationships between Blue- and Red-based Vegetation Indices and Leaf Area and Yield of Alfalfa. *Crop Sci.* **2007**, *47*, 2547–2556. [CrossRef]
30. Duncan, L.; Miller, B.; Shaw, C.; Graebner, R.; Moretti, M.L.; Walter, C.; Selker, J.; Udell, C. Weed Warden: A low-cost weed detection device implemented with spectral triad sensor for agricultural applications. *HardwareX* **2022**, *11*, e00303. [CrossRef]

31. Basyuni, M.; Wirasatriya, A.; Iryanthony, S.B.; Amelia, R.; Slamet, B.; Sulistiyono, N.; Pribadi, R.; Sumarga, E.; Eddy, S.; Al Mustaniroh, S.S.; et al. Aboveground biomass and carbon stock estimation using UAV photogrammetry in Indonesian mangroves and other competing land uses. *Ecol. Inform.* **2023**, *77*, 102227. [CrossRef]
32. Wan, L.; Zhang, J.; Dong, X.; Du, X.; Zhu, J.; Sun, D.; Liu, Y.; He, Y.; Cen, H. Unmanned aerial vehicle-based field phenotyping of crop biomass using growth traits retrieved from PROSAIL model. *Comput. Electron. Agric.* **2021**, *187*, 106304. [CrossRef]
33. Xu, T.; Wang, F.; Shi, Z.; Miao, Y. Multi-scale monitoring of rice aboveground biomass by combining spectral and textural information from UAV hyperspectral images. *Int. J. Appl. Earth Obs. Geoinf.* **2024**, *127*, 103655. [CrossRef]
34. Taşan, S.; Cemek, B.; Taşan, M.; Cantürk, A. Estimation of eggplant yield with machine learning methods using spectral vegetation indices. *Comput. Electron. Agric.* **2022**, *202*, 107367. [CrossRef]
35. Freitas, R.G.; Pereira, F.R.S.; Dos Reis, A.A.; Magalhães, P.S.G.; Figueiredo, G.K.D.A.; do Amaral, L.R. Estimating pasture aboveground biomass under an integrated crop-livestock system based on spectral and texture measures derived from UAV images. *Comput. Electron. Agric.* **2022**, *198*, 107122. [CrossRef]
36. Zhang, H.; Tang, Z.; Wang, B.; Meng, B.; Qin, Y.; Sun, Y.; Lv, Y.; Zhang, J.; Yi, S. A non-destructive method for rapid acquisition of grassland aboveground biomass for satellite ground verification using UAV RGB images. *Glob. Ecol. Conserv.* **2022**, *33*, e01999. [CrossRef]
37. Li, J.; Schachtman, D.P.; Creech, C.F.; Wang, L.; Ge, Y.; Shi, Y. Evaluation of UAV-derived multimodal remote sensing data for biomass prediction and drought tolerance assessment in bioenergy sorghum. *Crop J.* **2022**, *10*, 1363–1375. [CrossRef]
38. Rouse, J.W.; Haas, R.H.; Schell, J.A.; Deering, D.W. Monitoring vegetation systems in the great plains with ERTS. In Proceedings of the Third Earth Resources Technology Satellite-1 Symposium, Washington, DC, USA, 10–14 December 1973; pp. 309–317.
39. Shao, G.; Han, W.; Zhang, H.; Wang, Y.; Zhang, L.; Niu, Y.; Zhang, Y.; Cao, P. Estimation of transpiration coefficient and aboveground biomass in maize using time-series UAV multispectral imagery. *Crop J.* **2022**, *10*, 1376–1385. [CrossRef]
40. Liang, Y.; Kou, W.; Lai, H.; Wang, J.; Wang, Q.; Xu, W.; Wang, H.; Lu, N. Improved estimation of aboveground biomass in rubber plantations by fusing spectral and textural information from UAV-based RGB imagery. *Ecol. Indic.* **2022**, *142*, 109286. [CrossRef]